Itinerant Antiferromagnetism in RuO_2

T. Berlijn,[1,2] P. C. Snijders,[3,4] O. Delaire,[3,5] H.-D. Zhou,[4] T. A. Maier,[1,2] H.-B. Cao,[6] S.-X. Chi,[6] M. Matsuda,[6] Y. Wang,[3] M. R. Koehler,[7] P. R. C. Kent,[1,2] and H. H. Weitering[4,3]

[1]*Center for Nanophase Materials Sciences, Oak Ridge National Laboratory, Oak Ridge, Tennessee 37831, USA*
[2]*Computer Science and Mathematics Division, Oak Ridge National Laboratory, Oak Ridge, Tennessee 37831, USA*
[3]*Materials Science and Technology Division, Oak Ridge National Laboratory, Oak Ridge, Tennessee 37831, USA*
[4]*Department of Physics and Astronomy, The University of Tennessee, Knoxville, Tennessee 37996, USA*
[5]*Mechanical Engineering and Materials Science, Duke University, Durham, North Carolina 27708, USA*
[6]*Quantum Condensed Matter Division, Oak Ridge National Laboratory, Oak Ridge, Tennessee 37831, USA*
[7]*Department of Materials Science and Engineering, The University of Tennessee, Knoxville, Tennessee 37996, USA*

(Received 6 July 2016; published 15 February 2017)

Bulk rutile RuO_2 has long been considered a Pauli paramagnet. Here we report that RuO_2 exhibits a hitherto undetected lattice distortion below approximately 900 K. The distortion is accompanied by antiferromagnetic order up to at least 300 K with a small room temperature magnetic moment of approximately $0.05\mu_B$ as evidenced by polarized neutron diffraction. Density functional theory plus U (DFT + U) calculations indicate that antiferromagnetism is favored even for small values of the Hubbard U of the order of 1 eV. The antiferromagnetism may be traced to a Fermi surface instability, lifting the band degeneracy imposed by the rutile crystal field. The combination of high Néel temperature and small itinerant moments make RuO_2 unique among ruthenate compounds and among oxide materials in general.

DOI: 10.1103/PhysRevLett.118.077201

Theories of magnetism in 3d transition metal oxides (TMOs) are usually framed in the context of strong Coulomb repulsions and Hund's rule coupling in the 3d orbitals of the transition metal cation, and their covalent bonding with the oxygen 2p orbitals. Strong on-site electron interactions tend to inhibit double occupancy of the 3d orbital and the overall Coulomb energy of the crystal is lowered by localizing the valence charge of the cation. Covalent bonding delocalizes the d-electron charge and thus lowers the kinetic energy. The former mechanism favors the formation of local magnetic moments while the latter decreases the moment but increases the exchange coupling between the moments through virtual hopping processes. In particular, the anion-mediated Kramers-Anderson "superexchange" between half-filled 3d orbitals often gives rise to strong antiferromagnetism. Many 3d transition metal oxides can be classified as antiferromagnetic Mott insulators where the on-site Coulomb repulsion U exceeds the electronic band width W.

4d TMOs generally have significantly greater band widths and smaller U, due to the larger spatial extent of the 4d orbitals. With U and W being more-or-less comparable in magnitude [1–3], they are representative of the less well-understood intermediate coupling regime. Without clear evidence of local moment formation and/or magnetic ordering, many of them are considered to be metallic Pauli paramagnets. The ruthenate family is a notable exception and features a variety of magnetically ordered phases. The best-known examples are the Ca-based Ca_2RuO_4 and $Ca_3Ru_2O_7$, and Sr-based $Sr_3Ru_2O_7$, $Sr_4Ru_3O_{10}$, and $SrRuO_3$ perovskites, featuring antiferromagnetic insulating and ferromagnetic metallic ground states, respectively [4]. Their magnetic ordering temperatures are generally low, although recently $SrRu_2O_6$ has been reported to host high-temperature antiferromagnetism [5] with a Néel temperature $T_N \sim 563$ K [3,6]. Ruthenium dioxide (RuO_2), on the other hand, has been thought to fall in line with other binary 4d transition metal oxides [7]; it is a good metal [8] and believed to be Pauli paramagnetic [9]. From the point of view of correlated electron physics and magnetism, RuO_2 seems to be one of the least interesting 4d TMOs. From a technology perspective, however, RuO_2 is by far one of the most important oxides. It has numerous applications in electro- and heterogeneous catalysis, as electrode material in electrolytic cells, supercapacitors, batteries and fuel cells, and as diffusion barriers in microelectronic devices [10]. It owes its usefulness in part to its relatively high electrical conductivity combined with its excellent thermal and chemical stability [11]. For the technological applications little attention has been paid to the potential role of magnetism (with the exception of Ref. [12]), presumably because magnetism is generally believed to be nonexistent in bulk RuO_2.

In this Letter we report on the finding that RuO_2 is distorted from the rutile symmetry ($P4_2/mnm$) and exhibits antiferromagnetic order up to at least 300 K. Our DFT + U calculations show that for a reasonable range of local interactions, the moments within the Ru_2O_4 rutile unit cell strongly prefer to align antiferromagnetically. The predicted magnetic order is confirmed with polarized neutron scattering experiments that show structurally forbidden peaks with a significantly decreased non-spin-flip to spin-flip intensity ratio. We conjecture that the relatively

high Néel temperature can be attributed to the existence of half-filled t_{2g} orbitals, in conjunction with a fairly large band width, similar to the recently reported case of $SrTcO_3$. Both materials can be described as strongly covalent intermediate coupling systems. An important distinction, however, is that RuO_2 is metallic and that its magnetism may be traced to a Fermi surface instability, whereas $SrTcO_3$ has been predicted to be a narrow gap insulator. These findings not only provide new insights into the origins of antiferromagnetism in the intermediate coupling regime, but may also have important ramifications for the understanding of the remarkable properties that make RuO_2 attractive for technological applications.

We begin our investigation of magnetism in RuO_2 with a DFT analysis (see Ref. [13] for technical details). The majority of theoretical investigations considered bulk RuO_2 to be nonmagnetic. However, almost none of these studies considered the effects of on-site Coulomb interactions among the Ru $4d$ orbitals. Although these interactions are expected to be weaker than those in $3d$ TMOs, they should not be ignored. Indeed, Ru L_{23} x-ray-absorption spectra in combination with crystal-field-multiplet calculations indicated the importance of Coulomb interactions in RuO_2 [30]. Ru $3d$ core-level x-ray photoemission spectroscopy on RuO_2 was found to be most consistent with a dynamical mean field theory treatment of the single band Hubbard model, when U is taken to be 1.8 eV compared to a bandwidth W of 3.6 eV [1]. Since interactions always play a critical role in magnetism it is imperative that we include their effects in our theoretical investigation. To this end, we employ the PBE+U functional.

The DFT results are summarized in Fig. 1(a). First, we find that even for a weak U of 1.2 eV, the Ru moments within the rutile unit cell prefer to align antiferromagnetically [see Fig. 1(b)]. With increasing U, the energy of the AFM configuration decreases relative to that of the nonmagnetic structure. For $U = 4$ eV, the system is no longer metallic and exhibits a band gap of about 0.5 eV,

(a)

U=1.2eV	E_{tot}(meV)	$\lvert M_{Ru}\rvert(\mu_B)$	E_{gap}(eV)	DOS_{EF} (eV^{-1})
AFM	0	0.742	0	2.80
NM	3	0	0	2.93

U=2.0eV	E_{tot}(meV)	$\lvert M_{Ru}\rvert(\mu_B)$	E_{gap}(eV)	DOS_{EF} (eV^{-1})
AFM	0	1.183	0	1.00
NM	72	0	0	2.40

U=4.0eV	E_{tot}(meV)	$\lvert M_{Ru}\rvert(\mu_B)$	E_{gap}(eV)	DOS_{EF} (eV^{-1})
AFM	0	1.594	0.5	0
NM	405	0	0	1.03
FM	408	1.687	0	0.80

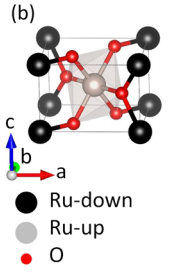

FIG. 1. (a) Total energy per Ru in meV, Ru magnetic moments within the rutile unit cell in μ_B, band gap in eV, and density of states at the Fermi energy per eV per Ru, of the antiferromagnetic (AFM), the nonmagnetic (NM), and the ferromagnetic (FM) configurations calculated with PBE + U. (b) Atomic and antiferromagnetic structure of bulk rutile RuO_2 as predicted by DFT and confirmed by neutron diffraction.

contradicting the experimental fact that RuO_2 is a metal [8]. For $U = 2$ eV we find that the AFM configuration is more stable than the nonmagnetic one by a significant 72 meV per Ru atom, while still retaining a sizable density of states at the Fermi level of about 1 eV^{-1} per Ru atom. The AFM configuration was reproduced using hybrid functionals [13,31]. Apparently it requires an intermediate range of interaction strengths in RuO_2 to be simultaneously AFM and metallic. We also considered the influence of the spin-orbit coupling, which we found to have a small effect on the electronic band structure and to only make small quantitative changes in the relative total energies of the magnetic configurations [13]. Ferromagnetic configurations turned out to be unstable or high in energy.

To validate the DFT results, we synthesized RuO_2 single crystals via vapor transport in flowing oxygen, and subjected those crystals to extensive x-ray diffraction (XRD), neutron scattering, and magnetic susceptibility investigations [13]. For the perfect rutile structure, non-magnetic Ru contributions to the (hkl) Bragg reflection vanish when $h + k + l =$ odd. The non-magnetic oxygen contributions vanish when $h + l =$ odd and $k = 0$, or when $k + l =$ odd and $h = 0$. Indeed, the XRD data in Fig. 2(a), acquired at room temperature, show that the (100) Bragg peak is absent while the (200) and (111) peaks are clearly visible. On the other hand, room temperature unpolarized neutron diffraction data on a sample from the same crystal batch [Fig. 2(b)] clearly reveal significant scattering intensity at reciprocal lattice points with odd indices such as (100) and (300), but not at the (001)and (003) locations. This would be consistent with the AFM configuration found from DFT, but it could also imply the existence of a lattice distortion that would be invisible when using a conventional x-ray source.

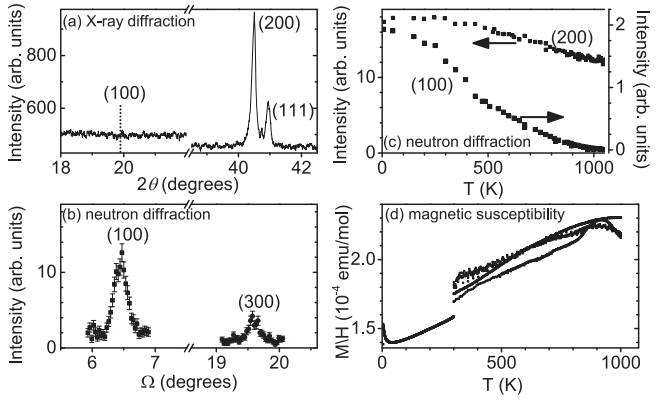

FIG. 2. (a) X-ray and (b) unpolarized neutron diffraction data taken at 295 K at the HB-3A instrument at the High Flux Isotope Reactor in Oak Ridge National Laboratory (HFIR/ORNL). (c) Temperature evolution of the integrated intensity of the nuclear (200) (left) and magnetic (100) (right) peak measured at the HB-3A and HB-3 instruments at HFIR/ORNL. (d) Magnetic susceptibility of different multigrain RuO_2 samples as a function of temperature.

In particular, the x-ray scattering cross section for light elements such as oxygen is very small. Interestingly, a polarized neutron scattering analysis of the (100) peak at 300 K [13], indicates that RuO_2 is both distorted and antiferromagnetic at room temperature. While the majority contribution to the (100) peak intensity seems to be structural in origin, it does contain a magnetic scattering contribution: the non-spin-flip to spin-flip intensity ratio R for the (200) peak is 12.8(2), whereas R for the (100) peak is 8.0 (2) [13]. While this magnetic scattering contribution equates to only a small moment of about $0.05\mu_B$ at room temperature [13], the presence of this magnetic moment is unambiguously demonstrated by the 60% larger R of the (200) peak as compared to the (100) peak. Given that at 300 K the (100) peak intensity is close to being saturated [cf. Fig. 2(c)], a significant increase of the moment towards lower temperatures is unlikely.

The existence of room temperature antiferromagnetism is thus clearly established. However, the nature of the small lattice distortion is not understood. A symmetry analysis shows [13] that there are only two possible tetragonal subgroups of the rutile space group that could produce finite intensities for the forbidden reflections like (100) and (300). Yet, a full refinement of the unpolarized neutron diffraction data involving over one hundred reflections, clearly converges to the rutile symmetry and, consequently, overestimates the magnetic moments. [13] Attempts within DFT + U to find another total-energy minimum by breaking the rutile symmetry were unsuccessful [13]. At this point we are therefore not able to capture the nature of the distortion with a model that is consistent with the unpolarized neutron and x-ray scattering experiments, or the DFT + U simulations, and leave this question for future investigations. The absence of the (001) reflection in neutron scattering implies the lack of a structural deformation along the c direction and alignment of the magnetic moments along the rutile c axis (the unpolarized neutron cross section vanishes when the scattering vector is parallel to the magnetic moment). We note that the experimental magnetic moment of $\sim 0.05\mu_B$ from polarized neutron scattering is much smaller than the one predicted by DFT. Such discrepancies between DFT and experiment are quite common in metallic antiferromagnets, such as, for example, the Fe based superconductors [32,33], and probably reflect the inability of the static mean field DFT to capture charge and spin fluctuations in time and space.

Figure 2(c) shows the full temperature dependence of the (100) and (200) diffraction intensities. The (100) peak vanishes near 1000 K while the (200) peak persists to higher temperature and diminishes in intensity according to the Debye-Waller factor. This rules out multiple scattering as the origin of the (100) reflection, because the temperature dependences of the (100) and (200) peaks are clearly different. The concave temperature dependence of the (100) peak intensity furthermore suggests that the magnetic and/or structural ordering is fairly short range. This is consistent with the Lorentzian line shape of the (100) peak, as opposed to the Gaussian line shape of the (200) reflection [13].

The presence of room temperature antiferromagnetism goes against the current lore that RuO_2 is a Pauli paramagnet. This general belief probably stems from the early work by Ryden *et al.* [9] that concluded Pauli paramagnetism from the quadratic temperature dependence of the magnetic susceptibility within 4–300 K. However, older measurements of the magnetic susceptibility [34,35] were performed for much larger temperature ranges up to 1000 K and demonstrated instead a linear increase as a function of temperature. We repeated those measurements while ramping the temperature continuously from 4 to 300 K and from 300 to 1000 K. The results are presented in Fig. 2(d). The value of 1.7×10^{-4} emu/mol (300 K) is in good agreement with previous reports [9,34,35]. The 30% rise of the magnetic susceptibility with increased temperature from 300 to 1000 K is also in excellent agreement with Fletcher *et al.* [35], the only study that measured up to 1000 K. Our measurements, however, either produce a clear, broad maximum in the susceptibility or a significant leveling at the highest temperature, consistent with the presence of short-range ordering. Because of the extreme difficulty in measuring small magnetic signals at such high temperature, which is near the limit of our instrument capability, as well as the possible loss of oxygen, different crystals produce slightly different behavior above 850 K. It is possible that this changing magnetic behavior above 900 K is related to the vanishing of the (100) peak and its underlying magnetic and/or structural order.

Given the itinerant nature of the conduction electrons in RuO_2, antiferromagnetism possibly originates from a spin density wave instability of the Fermi surface. To explore this possibility, we calculate the Lindhard response function. To this end, we first map the first-principles electronic structure from a nonmagnetic DFT calculation (with $U = 0$) onto a low energy effective model that only contains the Ru $4d$ orbital degrees of freedom. Specifically, we perform a Wannier transformation of the 2×5 Ru $4d$ bands within the $[-2, 6.5]$ eV energy window. The resulting tight binding Hamiltonian then allows us to efficiently compute the Lindhard response $\chi_0(q)$ as a function of the momentum q according to

$$\chi_0[q] = \sum_k \left\{ \sum_{st\mu\nu} \frac{\langle s|\mu k\rangle\langle \mu k|t\rangle\langle t|\nu k+q\rangle\langle \nu k+q|s\rangle}{E_\nu(k+q) - E_\mu(k)} \times \left(f[E_\nu(k+q)] - f[E_\mu(k)]\right) \right\}, \quad (1)$$

where s, $t\,(\mu, \nu)$ denote the orbital (band) indices, respectively, k, $k+q$ the momenta, and $f[E]$ the Fermi distribution function at energy E. As shown in Fig. 3(a), the response function χ_0 is peaked at $q = (2\pi, 0, 0)$ and $q = (0, 2\pi, 0)$ with a value of roughly 1.4 eV^{-1}. Therefore,

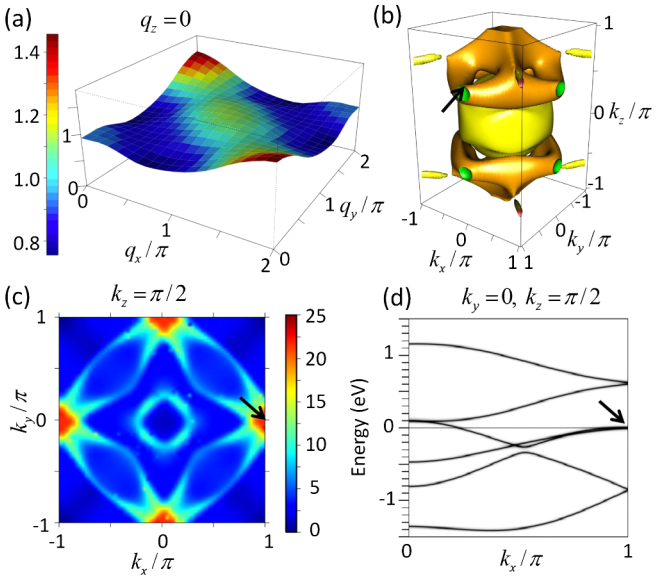

FIG. 3. (a) Lindhard response function $\chi_0[q]$ in eV^{-1}. (b) Fermi surface. (c) Momentum resolved contribution to $\chi_0[q = (2\pi, 0, 0)]$. (d) Band structure at $k_y = 0$ and $k_z = 0.5\pi$ along the k_x direction. Black arrow in various panels indicates one of eight nested hot spots.

within the random phase approximation [36] the interacting response function, given by $\chi = \chi_0/(1 - U\chi_0)$, will diverge for interactions larger than $\mathrm{U} \approx (1/1.4)$ eV driving the system towards a spin density wave instability.

Such a spin density wave (or AFM) modulation would produce magnetic reflections at the (100) and (010) locations in reciprocal space, exactly as predicted by DFT and observed experimentally. Figure 3(c) shows the crystal momentum resolved contribution to the magnetic susceptibility, obtained from evaluating the term in the curly bracket in Eq. (1) as a function of crystal momentum k for the fixed momentum $q = (2\pi, 0, 0)$. From the heat map in Fig. 3(c) we see that the dominating contributions originate from states near $(\pi, 0, \pi/2)$ and symmetry related points. These "hot spots" are located at the neck-shaped regions of the Fermi surface as indicated by the black arrows in Fig. 3(b). The energy bands near these k points have very low Fermi velocities [Fig. 3(d)] and thus contribute a large density of states to the magnetic instability. The hot spots are folded on top of one another via translation by a reciprocal lattice vector. This can be seen in Fig. 3(d). Note that the bands at the hot spot location are doubly degenerate, which is a consequence of the rutile symmetry. This degeneracy is lifted by antiferromagnetism and as a consequence of the hot spots being folded on top of each other, the magnetic unit cell equals the structural unit cell. This hot spot mechanism differs from the classical example of chromium [37] in which nesting takes place between large parallel sheets of Fermi surface, but is analogous to that being proposed for charge density waves in $2H$-$NbSe_2$ [38]. Whether the Fermi surface hot spots in RuO_2 are capable of driving the antiferromagnetism or rather play an assisting role, remains an open question—one that is an integral part of the longstanding debate on itinerant versus localized magnetism in metallic systems [39,40].

The discovery of AFM in RuO_2 and particularly its relatively high Néel temperature (≥ 300 K) is significant because metallic AFM oxides are rare [41,42], and their ordering temperatures are generally low. For example, within the $3d$ series, $CaCrO_3$ and $Sr_{0.99}Ce_{0.01}MnO_3$ have a T_N of 90 [43] and 220 K [44], respectively. In the $4d$ series, the ruthenates $Ca_3Ru_2O_7$ and Na-doped $CaRuO_3$ display antiferromagnetism at $T_N = 56$ and 70 K, respectively, significantly lower than that of RuO_2 [45,46], and they are borderline insulating. Indeed, the recent discoveries of AFM with high T_N in $4d$ transition metal oxides were made in semiconducting $SrRu_2O_6$ ($T_N \sim 563$ K) [3,5,6] and $SrTcO_3$ ($T_N = 1023$ K) [47]; the latter is theoretically predicted to be insulating [2,47]. While the debate on itinerant versus localized magnetism in metallic systems [39,40] shows that it is difficult to determine the role of itineracy in AFM order, the robust metallicity, small moment, and high magnetic ordering temperature of RuO_2 places it in a regime that was hitherto not accessible in transition metal oxides.

The relatively high T_N in RuO_2 appears to be consistent with recent explanations of high temperature AFM in $SrTcO_3$ [2] and $SrRu_2O_6$ [3]. Here it was argued that T_N maximizes in a regime in which the ratio of the interaction U and the band width W is large enough to form robust magnetic moments, but small enough to allow for significant exchange interactions between those moments. Both high-T_N compounds share another important feature, namely, the existence of a $4d^3$ electron configuration. Since at T_N $SrTcO_3$ has the ideal perovskite symmetry (space group $Pm\bar{3}m$) [47], the three t_{2g} orbitals are degenerate and thus half filled. In $SrRu_2O_6$ the RuO_6 octahedra are stretched along the c axis, but the C_{3v} symmetry still protects the t_{2g} orbital degeneracy [48]. Hence, the 3 t_{2g} orbitals are also half filled. A simple chemical bonding picture by Moriya [49] explains why antiferromagnetism (localized or itinerant) is particularly stable at half filling: the majority spin states on one magnetic sublattice hybridize with the minority spin states on the other sublattice, and the resulting "chemical bond" is most stable at half filling while the stabilization energy is determined by the bandwidth.

At first sight, RuO_2 does not seem to match this picture as it has a $4d^4$ electron count. However, our orbital resolved density of states shows [13] that the $4d_{x^2-y^2}$ orbital is filled with two electrons and resides below E_F, leaving the remaining two t_{2g} orbitals half filled. Hence, the specific crystal field splitting of the edge-shared octahedra in the rutile structure ensures that the $4d_{xz}$ and $4d_{yz}$ t_{2g} orbitals that are relevant for the AFM order are formally half filled, similar to $SrTcO_3$ and $SrRu_2O_6$. An important distinction, however, is that RuO_2 is a good metal whereas $SrTcO_3$ is

theoretically predicted to be insulating [2,47] and $SrRu_2O_6$ has been determined to be semiconducting from resistivity measurements. [5] The unique combination of good metallicity and high temperature AFM in RuO_2 will allow for a more complete benchmarking of theoretical models describing the interplay between magnetism and metallicity in oxide materials.

Our discovery of antiferromagnetism in a strongly metallic binary oxide material also calls for the reevaluation of the magnetic properties of other 4*d* and 5*d* metallic oxide systems. Many of these materials already are of technological importance, often as catalyst or other chemical applications, but the existence of itinerant antiferromagnetism in this class of materials would open up a new realm of possibilities, specifically in light of recent developments in antiferromagnetic-metal spintronics [50]. Here it may be needed to enhance the magnetic properties, such as the moment, via, e.g., alloy substitution or dimensional confinement.

We thank Veerle Keppens for the use of her laboratory equipment. The research was supported by the U.S. Department of Energy, Office of Science, Basic Energy Sciences, Materials Sciences and Engineering Division (T. B., P. C. S., O. D., Y. W., P. R. C. K., H. H. W.). Work by T. A. M. (response function calculation) was performed at the Center for Nanophase Materials Sciences, a DOE Office of Science user facility. H. D. Z. (crystal growth, XRD and low temperature susceptibility measurements) acknowledges support from NSF-DMR-1350002. M. R. K. (high temperature susceptibility measurements) acknowledges support from the Gordon and Betty Moore Foundations EPiQS Initiative through Grant No. GBM F4416. Research at ORNL's High Flux Isotope Reactor (H. B. C., M. M., S. X. C.) was sponsored by the Scientific User Facilities Division, Office of Basic Energy Sciences, U.S. Department of Energy. This research used resources of the National Energy Research Scientific Computing Center, a DOE Office of Science User Facility supported by the Office of Science of the U.S. DOE under Contract No. DE-AC02-05CH11231.

T. B. and P. C. S. contributed equally to this work.

[1] H.-D. Kim, H.-J. Noh, K. H. Kim, and S.-J. Oh, Phys. Rev. Lett. **93**, 126404 (2004).
[2] J. Mravlje, M. Aichhorn, and A. Georges, Phys. Rev. Lett. **108**, 197202 (2012).
[3] W. Tian, C. Svoboda, M. Ochi, M. Matsuda, H. B. Cao, J.-G. Cheng, B. C. Sales, D. G. Mandrus, R. Arita, N. Trivedi, and J.-Q. Yan, Phys. Rev. B **92**, 100404(R) (2015).
[4] G. Cao, C. S. Alexander, S. McCall, J. E. Crow, and R. P. Guertin, Mater. Sci. Eng. B **63**, 76 (1999).
[5] C. I. Hiley, M. R. Lees, J. M. Fisher, D. Thompsett, S. Agrestini, R. I. Smith, and R. I. Walton, Angew. Chem., Int. Ed. **53**, 4423 (2014).
[6] C. I. Hiley, D. O. Scanlon, A. A. Sokol, S. M. Woodley, A. M. Ganose, S. Sangiao, J. M. De Teresa, P. Manuel, D. D. Khalyavin, M. Walker, M. R. Lees, and R. I. Walton, Phys. Rev. B **92**, 104413 (2015).
[7] L. F. Mattheiss, Phys. Rev. B **13**, 2433 (1976).
[8] H. Schäfer, G. Schneidereit, and W. Gerhardt, Z. Anorg. Allg. Chem. **319**, 327 (1963).
[9] W. D. Ryden and A. W. Lawson, J. Chem. Phys. **52**, 6058 (1970).
[10] H. Over, Chem. Rev. **112**, 3356 (2012).
[11] S. Trasatti, *Electrodes and Conductive Metallic Oxides* (Elsevier, New York, 1980).
[12] E. Torun, C. M. Fang, G. A. de Wijs, and R. A. de Groot, J. Phys. Chem. C **117**, 6353 (2013).
[13] See Supplemental Material at http://link.aps.org/supplemental/10.1103/PhysRevLett.118.077201 for technical details, which includes Refs. [14–29].
[14] Y. S. Huang, H. L. Park, and F. H. Pollak, Mater. Res. Bull. **17**, 1305 (1982).
[15] B. C. Chakoumakos, H. B. Cao, F. Ye, A. D. Stoica, M. Popovici, M. Sundaram, W. Zhou, J. S. Hicks, G. W. Lynn, and R. A. Riedel, J. Appl. Crystallogr. **44**, 655 (2011).
[16] J. Rodriguez-Carvajal, Physica B (Amsterdam) **192**, 55 (1993)
[17] International Tables for Crystallography, http://it.iucr.org/Ab/ch7o1v0001/sgtable7o1o136/.
[18] P. E. Blöchl, Phys. Rev. B **50**, 17953 (1994).
[19] G. Kresse and J. Hafner, Phys. Rev. B **48**, 13115 (1993).
[20] G. Kresse and J. Furthmüller, Phys. Rev. B **54**, 11169 (1996).
[21] G. Kresse and D. Joubert, Phys. Rev. B **59**, 1758 (1999).
[22] S. L. Dudarev, G. A. Botton, S. Y. Savrasov, C. J. Humphreys, and A. P. Sutton, Phys. Rev. B **57**, 1505 (1998).
[23] A. A. Mostofi, J. R. Yates, G. Pizzi, Y. S. Lee, I. Souza, D. Vanderbilt, and N. Marzari, Comput. Phys. Commun. **185**, 2309 (2014).
[24] W. Ku, H. Rosner, W. E. Pickett, and R. T. Scalettar, Phys. Rev. Lett. **89**, 167204 (2002).
[25] V. Eyert, Ann. Phys. **11**, 650 (2002).
[26] C. E. Boman, Acta Chem. Scand. **24**, 116 (1970).
[27] P. J. Stephens, F. J. Devlin, C. F. Chabalowski, and M. J. Frisch, J. Phys. Chem. **98**, 11623 (1994).
[28] A. D. Becke, J. Chem. Phys. **98**, 5648 (1993).
[29] K.-P. Bohnen, R. Heid, O. de la Peña Seaman, B. Renker, P. Adelmann, and H. Schober, Phys. Rev. B **75**, 092301 (2007).
[30] Z. Hu, H. von Lips, M. S. Golden, J. Fink, G. Kaindl, F. M. F. de Groot, S. Ebbinghaus, and A. Reller, Phys. Rev. B **61**, 5262 (2000).
[31] Y. Ping, G. Galli, and W. A. Goddard, J. Phys. Chem. C **119**, 11570 (2015).
[32] N. Mannella, J. Phys. Condens. Matter **26**, 473202 (2014).
[33] Y.-T. Tam, D.-X. Yao, and W. Ku, Phys. Rev. Lett. **115**, 117001 (2015).
[34] A. N. Guthrie and L. T. Bourland, Phys. Rev. **37**, 303 (1931).
[35] J. M. Fletcher, W. E. Gardner, B. F. Greenfield, M. J. Holdoway, and M. H. Rand, J. Chem. Soc. A, 653 (1968).
[36] S. Graser, T. A. Maier, P. J. Hirschfeld, and D. J. Scalapino, New J. Phys. **11**, 025016 (2009).
[37] E. Fawcett, Rev. Mod. Phys. **60**, 209 (1988).

[38] S. V. Borisenko, A. A. Kordyuk, V. B. Zabolotnyy, D. S. Inosov, D. Evtushinsky, B. Büchner, A. N. Yaresko, A. Varykhalov, R. Follath, W. Eberhardt, L. Patthey, and H. Berger, Phys. Rev. Lett. **102**, 166402 (2009).
[39] E. P. Wohlfarth, J. Magn. Magn. Mater. **7**, 113 (1978).
[40] T. Moriya and Y. Takahashi, Annu. Rev. Mater. Sci. **14**, 1 (1984).
[41] P. A. Bhobe, A. Chainani, M. Taguchi, R. Eguchi, M. Matsunami, T. Ohtsuki, K. Ishizaka, M. Okawa, M. Oura, Y. Senba, H. Ohashi, M. Isobe, Y. Ueda, and S. Shin, Phys. Rev. B **83**, 165132 (2011).
[42] G. Zhang, Y. Wang, Z. Cheng, Y. Yan, C. Peng, C. Wang, and S. Dong, Phys. Chem. Chem. Phys. **17**, 12717 (2015).
[43] A. C. Komarek, S. V. Streltsov, M. Isobe, T. Möller, M. Hoelzel, A. Senyshyn, D. Trots, M. T. Fernández-Díaz, T. Hansen, H. Gotou, T. Yagi, Y. Ueda, V. I. Anisimov, M. Grüninger, D. I. Khomskii, and M. Braden, Phys. Rev. Lett. **101**, 167204 (2008).
[44] H. Sakai, S. Ishiwata, D. Okuyama, A. Nakao, H. Nakao, Y. Murakami, Y. Taguchi, and Y. Tokura, Phys. Rev. B **82**, 180409(R) (2010).
[45] G. Cao, S. McCall, J. E. Crow, and R. P. Guertin, Phys. Rev. Lett. **78**, 1751 (1997).
[46] M. Shepard, G. Cao, S. McCall, F. Freibert, and J. E. Crow, J. Appl. Phys. **79**, 4821 (1996).
[47] E. E. Rodriguez, F. Poineau, A. Llobet, B. J. Kennedy, M. Avdeev, G. J. Thorogood, M. L. Carter, R. Seshadri, D. J. Singh, and A. K. Cheetham, Phys. Rev. Lett. **106**, 067201 (2011).
[48] D. Wang, W.-S. Wang, and Q.-H. Wang, Phys. Rev. B **92**, 075112 (2015).
[49] T. Moriya, Solid State Commun. **2**, 239 (1964).
[50] B. G. Park, J. Wunderlich, X. Martí, V. Holý, Y. Kurosaki, M. Yamada, H. Yamamoto, A. Nishide, J. Hayakawa, H. Takahashi, A. B. Shick, and T. Jungwirth, Nat. Mater. **10**, 347 (2011).